



LAFAYETTE

SENIOR HONORS THESIS

DEPARTMENT OF MECHANICAL ENGINEERING

---

## Interaction of Cavity Frequencies in Supersonic Combustible Flow

---

*Author:*

D. Mac JONES

*Advisor:*

Dr. Tobias ROSSMANN

Thesis Committee:

**Dr. Tobias Rossmann**, Chair

Mechanical Engineering

**Dr. Daniel Sabatino**

Mechanical Engineering

**Dr. James Schaefer**

Chemical and Biomolecular Engineering

*A thesis submitted in fulfillment of the requirements  
for Honors in Mechanical Engineering  
in the*



April 2016

# **Declaration of Authorship**

I, D. Mac JONES, declare that this thesis titled, 'Interaction of Cavity Frequencies in Supersonic Combustible Flow' and the work presented in it are my own. I confirm that:

- This work was done wholly or mainly while in candidature for a research degree at this University.
- Where any part of this thesis has previously been submitted for a degree or any other qualification at this College or any other institution, this has been clearly stated.
- Where I have consulted the published work of others, this is always clearly attributed.
- Where I have quoted from the work of others, the source is always given. With the exception of such quotations, this thesis is entirely my own work.
- I have acknowledged all main sources of help.
- Where the thesis is based on work done by myself jointly with others, I have made clear exactly what was done by others and what I have contributed myself.

Signed:

---

Date:

---

*“60% of the time, it works every time.”*

Brian Fantana

*Abstract*

**Interaction of Cavity Frequencies in Supersonic  
Combustible Flow**

by D. Mac JONES

LAFAYETTE COLLEGE

Honors in Mechanical Engineering

The Thesis Abstract is written here (and usually kept to just this page or so . . . )

## *Acknowledgements*

The acknowledgements and the people to thank go here, don't forget to include your project advisor...

# Contents

|   |      |
|---|------|
| <b>Declaration of Authorship</b>              | i    |
| <b>Abstract</b>                               | iii  |
| <b>Acknowledgements</b>                       | iv   |
| <b>Contents</b>                               | v    |
| <b>List of Figures</b>                        | vii  |
| <b>List of Tables</b>                         | viii |
| <b>Abbreviations</b>                          | ix   |
| <b>Physical Constants</b>                     | x    |
| <b>Symbols</b>                                | xi   |
| <br>  |      |
| <b>1 Introduction</b>                         | 1    |
| 1.1 Motivation . . . . .                      | 1    |
| 1.1.1 Phase 1 . . . . .                       | 4    |
| 1.1.2 Phase 2 . . . . .                       | 4    |
| 1.1.3 Phase 3 . . . . .                       | 5    |
| <b>2 Theory</b>                               | 7    |
| 2.1 Cavity Flame-holding . . . . .            | 7    |
| 2.2 Cavity Acoustics . . . . .                | 7    |
| <b>3 Experimental Setup</b>                   | 9    |
| 3.1 Expansion Tube . . . . .                  | 9    |
| 3.1.1 Sections . . . . .                      | 9    |
| 3.1.2 Diaphragms . . . . .                    | 10   |
| 3.1.3 • . . . .                               | 13   |
| 3.2 Models . . . . .                          | 13   |
| 3.2.1 Design Choices . . . . .                | 13   |
| 3.2.2 Modular Design . . . . .                | 15   |
| 3.2.3 Implementation . . . . .                | 16   |
| 3.3 High Speed Pressure Transducers . . . . . | 16   |
| 3.3.1 Circuit . . . . .                       | 17   |

|          |  |           |
|----------|--|-----------|
| 3.3.2    | Implementation and Troubleshooting . . . . . | 17        |
| 3.4      | Infrared Sensor . . . . .                    | 17        |
| 3.4.1    | Design of System . . . . .                   | 18        |
| 3.4.2    | Set Up . . . . .                             | 18        |
| 3.4.3    | Absorption . . . . .                         | 19        |
| 3.4.4    | Emission . . . . .                           | 20        |
| 3.4.5    | Premature Ignition . . . . .                 | 21        |
| 3.5      | Schlieren Imaging . . . . .                  | 21        |
| <b>4</b> | <b>Experimentation</b>                       | <b>29</b> |
| 4.1      | Phase 1 . . . . .                            | 29        |
| 4.1.1    | Setup and Conditions . . . . .               | 29        |
| 4.2      | Phase 2 . . . . .                            | 29        |
| 4.2.1    | Setup and Conditions . . . . .               | 29        |
| <b>5</b> | <b>Experimental Results</b>                  | <b>30</b> |
| 5.1      | Phase 1 - Non-Combusting Tests . . . . .     | 30        |
| 5.1.1    | Schlieren . . . . .                          | 30        |
| 5.1.2    | IR . . . . .                                 | 30        |
| 5.2      | Combustion Tests . . . . .                   | 30        |
| 5.2.1    | Schlieren . . . . .                          | 30        |
| 5.2.2    | IR . . . . .                                 | 30        |
| <b>6</b> | <b>Future Work</b>                           | <b>31</b> |
| 6.1      | Phase 3 . . . . .                            | 31        |
| 6.2      | Suggestions for Other Improvements . . . . . | 31        |
| 6.2.1    | Pressure Transducers Within Cavity . . . . . | 31        |
| 6.2.2    | Fuel Injection into Cavities . . . . .       | 31        |
|          | <b>Bibliography</b>                          | <b>32</b> |

# List of Figures

|     |   |    |
|-----|---|----|
| 1.1 | Scramjet Diagram                              | 6  |
| 1.2 | Cavity-Actuated Mixing                        | 6  |
| 2.1 | Diagram of typical cavity                     | 8  |
| 3.1 | Annotated Expansion Tube                      | 23 |
| 3.2 | Cavity 3D Model                               | 24 |
| 3.3 | Cavity Model with Inserts                     | 24 |
| 3.4 | Circuit Diagram for Timer Counter Box         | 25 |
| 3.5 | Data Flow for High Speed Pressure Transducers | 26 |
| 3.6 | IR setup diagram                              | 27 |
| 3.7 | Labeled photograph of IR setup                | 27 |
| 3.8 | Schlieren Diagram                             | 28 |

# List of Tables

|   |    |
|---|----|
| 3.1 Diaphragm Burst Pressures . . . . . | 12 |
|---|----|

# Abbreviations

**FPS**   Frames Per Second

**L/D**   Length to Depth

**TTL**   Transistor Transistor Logic

# Physical Constants

Empirical Constant  $\alpha = 0.25$  (for cavities with L/D > 4)

Empirical Constant  $k = 0.57$  (for cavities with L/D > 4)

# Symbols

$m$  mode number

$M_\infty$  Freestream Mach Number

$U_\infty$  Freestream Velocity m/s

$\gamma_\infty$  Freestream Specific Heat Ratio

*For/Dedicated to/To my...*

# Chapter 1

## Introduction

### 1.1 Motivation

Scramjet engines are on the forefront of supersonic transportation development because of their simplicity and promising outlook for steady and reliable supersonic combustion. These engines differ from typical subsonic jet engines, as scramjets have no moving parts and simply rely on shock waves produced at these supersonic speeds to compress the intake air and provide the means for ignition. Shown in Figure 1.1 is a diagram of a typical scramjet engine.

One challenge facing the production of these engines is producing steady combustion. Much like keeping a match lit in a hurricane, keeping a flame stabilized at supersonic speeds is quite difficult. One proposed method of flame stabilization is a rectangular cavity. These cavities, are able provide a re-circulation zone with high temperatures and combustion radicals for strong combustion to occur. Many experimental studies have tested the flame-holding abilities of cavities in strong combustion cases [1–4]. Strong combustion occurs when the fuel-air mixture is optimized for efficient fuel burning. The

mixture in strong combustion cases occur in proper stoichiometric proportions. These studies focused on cavity dimensions and how the length to depth ratio, L/D, affects key ignition and flame holding characteristics, such as stagnation pressure, stagnation temperature, fuel air mixture, and residence time. Ben-Yakar concluded that with L/D ratios between 4 and 10, strong combustion can be sustained in these cavities for total enthalpy flight conditions of Mach 8, 10, and 13[2]. Also noted in several investigations is the presence of strong acoustic waves[5–10].

Similar to blowing air over an empty bottle to create a tone, the freestream air traveling over and interacting with these cavities produces acoustic waves. In these cavities, a shear layer develops between the high speed freestream and the slower, re-circulating air in the cavity. As the shear layer travels downstream, it begins to drop. By the time the shear layer reaches the downstream wall of the cavity, it has lowered to a point where the interaction of the shear layer with the downstream wall of the cavity produces strong pressure waves, which propagate upstream, ultimately resonating within the cavity.

Other experimental studies have investigated the acoustic properties of these cavities [5–9]. These investigations concluded that the acoustic waves generated by supersonic cavities produce several undesirable effects. One effect, investigated by McGregor is the induced drag associated with rectangular cavities. The effect of pressure waves within these cavities can increase the drag by as much as 250% [8]. These acoustic waves can also have an adverse effect on equipment and the crew. At low frequencies, the resonating acoustic waves can cause structural damage to the engine. At high frequencies, these waves can cause uneasiness in crew members [8].

Conclusions drawn from these investigations have led to the desire to suppress these acoustic waves. Suppressing these waves would reduce drag on the engine and cause

less damage to the engine or the crew. However, these acoustic waves could have the potential to assist in combustion when conditions for weak combustion are present. Weak combustion, as is studied in this investigation, is at lean fuel air mixture conditions. Sato et al.[10] investigated the enhancement of mixing due to acoustic waves. They concluded that mixing was enhanced by these acoustic waves and the rate of enhancement was controlled by the cavity's shape. However, the investigations performed by Sato et al. did not include the cavity as a flame-holder. The cavity was only used to produce the mixing enhancing acoustic waves.

One study, though, focused on the ability of cavity-induced acoustic waves to enhance mixing [? ]. Their experimental setup, as shown in Figure 1.2 shows that the wall-mounted cavities were used exclusively as acoustic wave generators to enhance the mixing of the freestream and the injected gas. Their study showed that the cavity acoustic waves produced had enough energy to enhance mixing. This study will attempt to combine the flame-holding characteristics of these cavities with the acoustic wave assisted mixing. The acoustic waves generated inside the cavity should have nearly the same strength as the waves that escaped the cavity in Sato's study.

Few, if any, experimental studies have investigated the acoustic properties of these cavities as they assist in mixing and the enhancement of combustion at lean conditions. This investigation is broken into three parts, which together will provide a clear interpretation of a cavity's suitability as an effective flame holder during weak combustion conditions.

### 1.1.1 Phase 1

The first part of the investigation isolated the acoustic properties of the cavities. The frequency of a cavity can be estimated using an empirical equation derived by Heller and Delfs [6], as shown in Equation 1.1. This equation is estimated to be able to predict the frequency within the cavity  $\pm 10\%$ [6].

$$f_m = \frac{m - \alpha}{\{M_\infty / \sqrt{1 + [(\gamma_\infty - 1)/2]M_\infty^2} + 1/k\}} \cdot \frac{U_\infty}{L} \quad (1.1)$$

Depending on the mode of the strongest acoustic waves, frequencies of these waves were expected to be between **FREQUENCY RANGE**. For this phase, three L/D ratios were investigated: 5, 7, and 9. From the equation, it can be seen that the frequency generated by the cavity is a function of the freestream test gas conditions and length of the cavity. Keeping the freestream conditions nearly identical while changing the length of the cavity produced different frequencies within the cavity. Data from these tests led to the direct comparison of the acoustic properties of the cavities, such as frequency and relative strength, as a function of cavity frequency. Also investigated at each of the L/D ratios was an angled downstream wall to observe the passive suppression of the normally present acoustic waves.

### 1.1.2 Phase 2

The second part of the investigation was used to isolate the combustion and flame-holding properties of the cavities.

### 1.1.3 Phase 3

The third part of the investigation has yet to be tested. This phase is used to observe the effect that the acoustic waves have on the flame-holding characteristics of the cavities in a non-stoichiometric fuel-air mixture. For these experiments, both flat and angled wall cavities will be tested at the same conditions. Shown by results of Phase 1, the angled walls do suppress the propagating acoustic waves within the cavity, so any observable differences between the results of the angled versus flat downstream wall will be assumed to be due to the cavity acoustics. Ideally, the results of these tests would be to show that the flat downstream wall, and thus the cavity acoustics, do enhance the mixing of the fuel and air, producing stronger combustion than the angled downstream wall. More details about Phase 3 are included in the Future Works section of this thesis, Chapter 6.

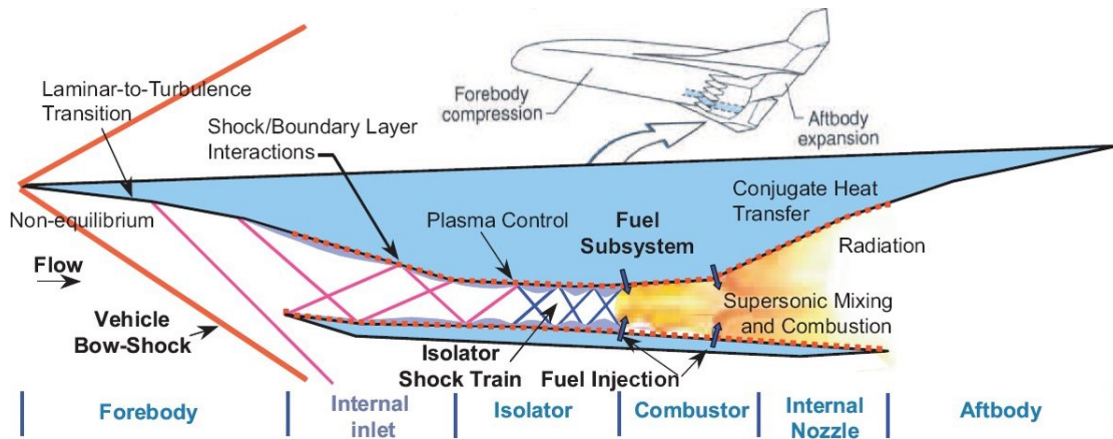


FIGURE 1.1: Diagram of a typical scramjet engine, showing shocks produced within the engine. [11]

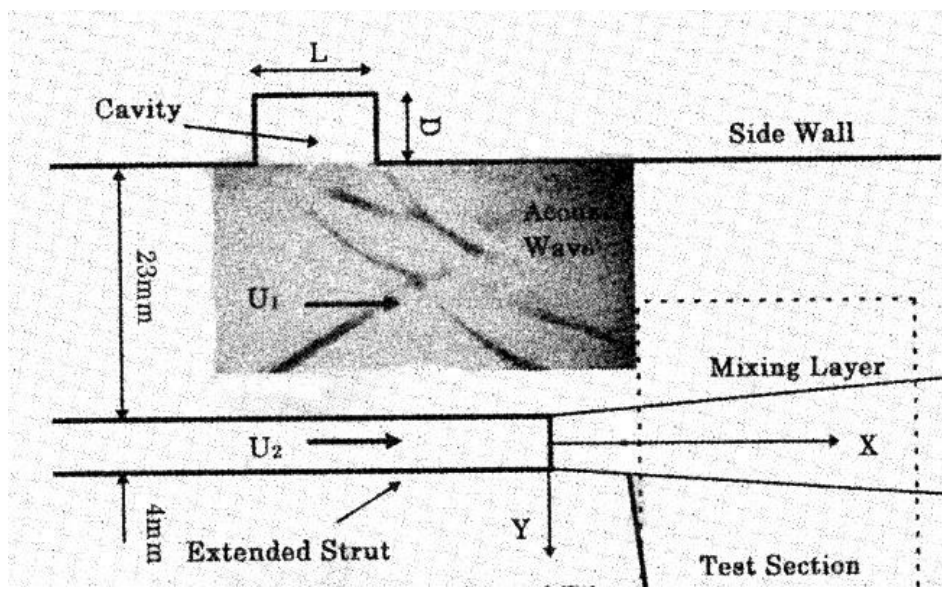


FIGURE 1.2: Mixing enhanced by acoustic waves produced by a side wall-mounted cavity [10]

# Chapter 2

## Theory

### 2.1 Cavity Flame-holding

### 2.2 Cavity Acoustics

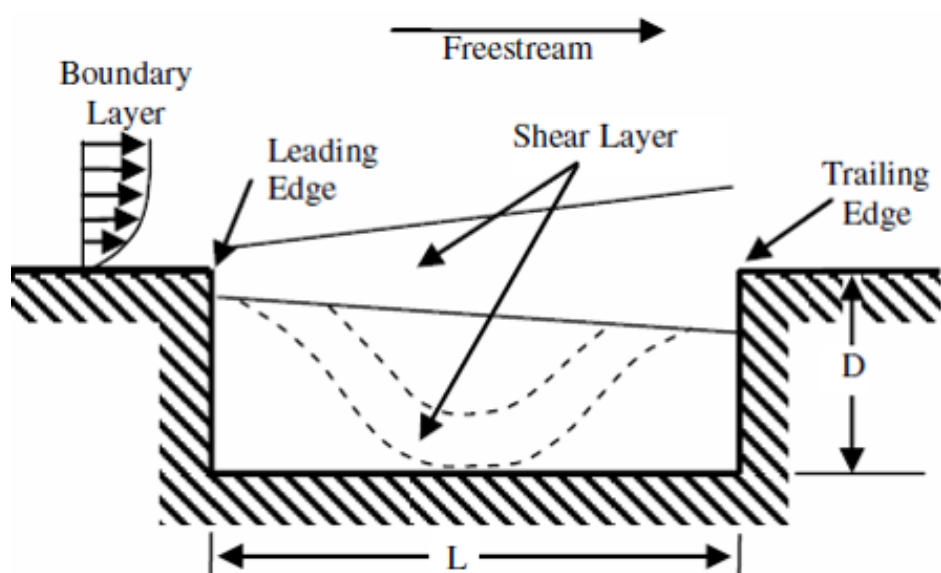


FIGURE 2.1: Typical hypersonic cavity schematic [12].

# Chapter 3

## Experimental Setup

### 3.1 Expansion Tube

The expansion tube is an impulse flow device similar to a shock tube. With an expansion tube, a high pressure gas is used to accelerate a volume of lower pressure gas to certain conditions required for supersonic testing. For the case of supersonic cavities, these conditions need to be similar to those found in the combustor of a scramjet engine. With the expansion tube at Lafayette College, Mach numbers between 2 and 4 have been attained, which correspond well with typical scramjet engine Mach numbers between [SCRAMJET mach numbers here](#).

#### 3.1.1 Sections

The expansion tube consists of four sections, which are highlighted in Figure 3.1. The four sections are: the driver, the double diaphragm, the driven, and the expansion, as listed from upstream to downstream. Initial conditions of the tube set by the operator determine test conditions within test section. These initial conditions include pressure

ratios between the sections as well as the gases used in the sections. Each section is divided by plastic diaphragms at the start of each tests. These diaphragms allow the sections to be filled to the different pressures with the different gases required for testing.

The driver section is contained at a high pressure at the start of a test. This section is rated to be filled up to 800 psi. Non-combusting tests performed were run with a driver pressure of 225 psi. With higher pressures, faster test velocities of the test gas can be achieved.

The double diaphragm serves as a starting mechanism for the experiments. It is filled to an intermediate pressure about half the driver pressure. This section is a very small volume (**place volume here**), which when vented, creates a large pressure drop across the most upstream diaphragm, causing it to break. The breaking of the diaphragm begins a chain reaction, starting the test.

Once the test begins, the test gas, which is contained in the driven section at a sub-atmospheric pressure, is accelerated by the driven gas. This gas travels down the tube, expanding and accelerating until it hits the last diaphragm between the driven and expansion sections. This last section differentiates an expansion tube from a shock tube. With the addition of the last diaphragm, the expansion section can be kept at an even lower pressure than the driven section. When the diaphragm between these sections break, the test gas experiences further expansion and acceleration, allowing faster freestream velocities and higher Mach numbers in the test section.

### 3.1.2 Diaphragms

To separate the four sections, plastic diaphragms were placed at the boundary between these sections. These diaphragms were used to keep a pressure differential between the

driver, double diaphragm, and driven sections. The pressure differential between these sections was a maximum of 120 psi for non-combusting tests. Another diaphragm was used to separate the test gas in the driver and the expansion gas in the expansion section. Depending on the test conditions, this diaphragm was required to withstand a maximum pressure differential of 1 psi.

Different thickness diaphragms were required, depending on the pressure differential between the sections. All diaphragms used for the driver and double diaphragm sections were cut from polycarbonate sheet. In order to determine the required diaphragm thickness, calculations were performed, utilizing known material properties and spherical pressure vessel relationships. Since the diaphragm is expected to expand to a near half sphere before breaking, a thin wall spherical pressure vessel relationship was used to determine the maximum pressure the plastic could withstand. This relationship, shown in Equation 3.1, was utilized to determine a range of thicknesses of the polycarbonate sheets to be used for different pressure conditions.

$$\sigma_{uts} = \frac{P r}{2t} \quad (3.1)$$

After initial testing of these diaphragms, it was determined this relationship provided an overestimation of about 185% for the breaking pressure of a specific thickness of diaphragm. Since the polycarbonate sheets come in certain stock thicknesses, several thicknesses were purchased and testing was performed to determine the breaking pressure of each diaphragm. For this testing, a 1/4" polycarbonate sheet was placed at the upstream end of the double diaphragm and the thinner test sample was placed at the downstream end of the double diaphragm. The double diaphragm was then filled slowly. When the downstream diaphragm broke, the highest pressure reached was recorded.

| Thickness (inches) | Trial 1 Burst Pressure (psi) | Trial 2 Burst Pressure (psi) |
|--------------------|------------------------------|------------------------------|
| 0.010              | 32                           | n/a                          |
| 0.015              | 60                           | n/a                          |
| 0.020              | 93                           | 92                           |
| 0.030              | 123                          | 125                          |
| 0.045              | 153                          | 163                          |
| 1/16               | 233                          | 274                          |
| 3/32               | 341                          | n/a                          |

TABLE 3.1: Diaphragm burst pressures at various thicknesses of polycarbonate sheets.

This procedure was repeated for other thicknesses of diaphragms. The results from these burst tests is shown in Table 3.1. A majority of the non-combusting tests run were at a driver pressure of 225 psi, so 0.045" diaphragms were selected, as they have a higher burst pressure than the pressure differential between the driven and the double diaphragm, but not higher than the differential between the driver and the driven sections. These diaphragms reliably broke for each test.

Occasionally, after a test was run, it was noticed that the pieces of the diaphragm completely broke off, sending these pieces down the tube. Having these large pieces of diaphragm sent down the tube is unwanted. These large pieces can cause serious damage to the model in the test section, as well as damage to other parts of the tube. During one test, a large piece of diaphragm struck the nose of the blunted cylinder model, causing severe damage to the pressure transducer located at the nose. It was also observed that pieces of diaphragm nicked the observation windows on the test section. These damages needed to be avoided, so one proposed solution to this problem was to score the diaphragms. A short, shallow incision on the outside of the plastic in an "X" pattern would create failure modes which the diaphragm should break along. These failure modes cause the diaphragm to petal, ideally opening as wide as the tube, with the entire diaphragm intact.

Burst tests were performed on several scored diaphragms of 0.045" thickness. This

scoring was performed by hand with a knife, applying light pressure. The resulting score appeared as deep scratches in an "X" pattern. The results of the tests showed no significant decrease in burst pressure. In fact, all of the tests showed a higher burst pressure for the scored diaphragms than for the not scored ones. This could be due to the scoring allowing the plastic to deform further before bursting. It could also be due to the plastic being from a different batch sheet than the plastic used for earlier burst tests. Regardless of the reason, the results showed that the scored diaphragms could still be used. It was also found that good petalling of the diaphragm occurred, with minimal, if any, loss of diaphragm pieces down the tube. Because of these results, scoring of the diaphragms has become a regular step in the setup of the tube for each test.

### 3.1.3 •

## 3.2 Models

For testing, a cavity model was designed and manufactured. The designed cavity, as shown in Figure 3.2, was designed to be mounted with the current mounting system in the test section. This mounting system consists of a rectangular upright with thru holes for shoulder bolts. The three holes seen in Figure 3.2 are in line with the existing holes in the mounting system. This allows one to swap out models in the test section quickly in between tests.

### 3.2.1 Design Choices

While designing the cavity, several choices had to be made about the geometry of the model as well as the features of the cavity. Brass was chosen as the material due to its

relatively low cost as well as its ability to be easily machined. Brass also holds up well to the conditions experienced in the test section during testing.

The overall size of the brass was chosen based on the size of the core flow exiting the tube into the test section as well as the requirement to be affixed to the existing mounting system. The size of the core flow coming out of the tube begins as about the diameter of the tube itself. However, it grows smaller as the length from the tube exit increases. It is important that the area of interest (the cavity) is contained entirely within this core flow. Knowing the cavity would sit a few inches from exit of the tube, a width of 2.5 inches was chosen for the brass. This would ensure that the core flow, at the time it hits the cavity, would entirely encapsulate the cavity. A total height of 1 inch was chosen because it allowed the rectangular hole for the mounting system to be machined to the correct depth that aligned the thru holes for the shoulder bolts. It was designed that after the rectangular hole was made in the brass, a thickness of 1/4 inch was left. This was chosen because the cavity exists relatively close to the mounting system and at least 1/8 inch of material needed to be left between the top of the mounting system and the bottom of the cavity to ensure the part could be machined without any issues.

The cavity itself was placed **THIS FAR AWAY FROM THE FRONT** in order to develop the flow over the flat plate. Flow conditions experienced by the cavity should match closely to flow conditions experienced in scramjet engines, including boundary layer conditions. For consistency with other researchers, as length of **THIS LENGTH** was chosen.

At the upstream end of the cavity model, there exists a wedge. Flow over a flat plate leading up to the cavity was desired. The wedge was designed in order to redirect any shock waves away from the cavity. These shock waves have the ability to adversely affect

test results if they interact with the cavity. Calculating shock wave angles for several wedge angles and calculating where the shocks would reflect off the walls of the test section, a wedge angle of **WEDGE ANGLE HERE** was chosen. This angle created a shock of **SHOCK ANGLE HERE**, which when reflected through the test section did not reflect into the cavity.

### 3.2.2 Modular Design

Because the acoustic properties are the main focus of this thesis, it was important to design a model in which these acoustic properties could change. Frequency is one main acoustic property that was chosen to be varied with these cavities. Using Heller and Delfs relationship, as stated previously, varying the length of the cavity would lead to different cavity frequencies [6]. However, the L/D is also an important parameter in the flame-holding characteristics of these cavities. Combining these need for various lengths with the need for certain range of L/D resulted in a modular design. For good flame-holding characteristics, a L/D between 4 and 10 has been shown to provide those characteristics [2]

For the modular design, a 1/8-inch deep, 1 5/8-inch long cavity was created, as shown in Figure 3.2. The length of the cavity was chosen so that inserts could be attached, decreasing the overall length of the cavity, and achieving the desired L/D. Six inserts were manufactured to create L/Ds of 5, 7, and 9. These inserts are shown relative to the base cavity in Figure 3.3. At each L/D, there was one insert with a flat wall and one insert manufactured with a 30° incline. This angled incline, as shown by Ben-Yakar [2], has the ability to suppress the acoustic waves. The angled wall does not allow the pressure waves to propagate within the cavity space. This allowed for the comparison of flame-holding abilities of the cavity with and without strong acoustic waves present

at each L/D. This modular design gave a relatively wide spectrum of cavity conditions to test with a relatively easy means of changing these conditions for each test.

### 3.2.3 Implementation

## 3.3 High Speed Pressure Transducers

Placed along the tube at various locations are piezoelectric pressure transducers. These pressure transducers provide both analog and digital data for each test run. The analog data allows for the observation of shock strength and the digital data allows for the calculation of shock velocity. The initial shock wave produced propagates down the tube. When the shock passes by one of these sensors, it registers as a very sharp increase in pressure. Knowing the time at which these shocks arrive at the various transducer locations, along with the location of the transducers relative to each other allows for the shock speed calculation.

In order to produce the digital signal required for the LabVIEW timer counter program to calculate the time between signals, a simple analog to digital circuit was designed. The design of the circuit was based off of previous work done by Helen Huches [13]. This circuit, as shown in Figure 3.4, produces a 5V signal when an analog voltage is higher than a certain threshold. This threshold reference voltage is determined by three potentiometers connected to the circuit. The three potentiometers allow three different reference voltages to be set for up to six pressure transducer signals. When the analog voltage is lower than this reference voltage, the output of the circuit is 0V. This allows the digital data acquisition card to read either a HIGH (5V) signal or a LOW (0V) signal and interpret that as a digital signal.

This digital signal is also used to trigger the camera to record. The LabVIEW program, once getting a signal from a specified pressure transducer will generate a 5V TTL pulse.

### 3.3.1 Circuit

### 3.3.2 Implementation and Troubleshooting

## 3.4 Infrared Sensor

Test time is important for the correlation of schlieren image data. Because the two systems are initiated simultaneously, the IR data corresponds easily to the image data. Knowing when the test gas reaches the model and for how long the test gas is flowing over the model allows for the extraction of frames that equate to just the test time. Although it is possible by inspection to see when the test gas arrives at the model, it is not always obvious. The arrival of the test gas produces shock waves at a different angle than the helium behind the incident shock wave, but this change in angle might not be very large, depending on the change in velocity. However, with the IR data, it can be closely estimated when the test gas should reach the model and for how long the model experiences the test gas.

The sensor used with the expansion tube at Lafayette is a Judson J10D series Indium Antemonide (InSb) sensor. These detectors have photovoltaic sensors that produce a current when exposed to infrared radiation. The sensor has the ability to be utilized for both absorption as well as emission sensing techniques. These techniques are explained in detail in a subsequent subsection.

### 3.4.1 Design of System

The alignment and placement of the various components is important for the proper collection of the IR light from the tube. The setup, as depicted in the diagram in Figure 3.6, includes a slit, a concave mirror, and a flat mirror. The slits affect the spacial resolution of the incoming signal. If the slits are too wide, the sensor captures some of the scattered light, which shows up as a gradual increase in signal. If the slits are too narrow, not enough light can be captured by the sensor to show a good signal. The slit width is still being fine-tuned for the system in place, but the typical width for the slits is between 1 and 3 mm.

The sensor itself has a circular pickup area of about 2mm in diameter. Because of this, the IR light from the tube needs to be focused. Once the light passes through the slits, it hits a concave mirror. This concave mirror, with a focal length of **insert focal length**, focuses the light to a small point, just about the size of the sensor. The flat mirror is used to collapse the system so it can fit in a relatively small area. The entire system is contained in a box, as shown in Figure 3.7. Since most of the testing is done during the day, the box is used to block out any ambient light from the room. The system is attached to the support structure of the tube by a 1/2" aluminum plate cantilever. Some bending, less than 1/16", is present at the end of the beam where the setup is supported, but it is not enough to affect the collection by the IR system.

### 3.4.2 Set Up

To achieve the sensitivity required for the sensor, the operating temperature of the IR detector is about 77K. Because of this, the detector must be cooled with liquid nitrogen. Using the funnel to avoid spillage of the liquid nitrogen onto the cable connections or

viewing window of the sensor, a few hundred milliliters were poured into the hole at the top of the sensor. When the sensor reaches the correct temperature, an eruption of cool gas occurs. It is important to wait until this eruption completes because the buildup of gas can cause the cap to blow off. Once the eruption subsides, the cap can be replaced to the top of the sensor and power can be supplied to the amplifier.

After power is supplied to the sensor through the amplifier, it is important to check that the system is aligned. Since the setup is attached to the support structure and not the tube itself, the recoil of the tube or the moving of the tube to replace diaphragms can alter the alignment of the window to the focusing mirror. To re-align the system, a stainless steel LED tube was constructed. This tube fits within the porthole on the back side of the tube, aligned with the port for the IR sensor. With the LED on and lined up with the inside wall of the tube, check the light source path. Be sure that the thin slit of red light hits the small sensor area. Adjust the flat mirror as needed to align the slit of red light with the IR sensor pickup area. Once the system is aligned, remove the LED tube and replace the plug in that port. The system at this point is aligned and ready for a test.

### **3.4.3 Absorption**

One method of data capturing that can be used is infrared absorption. The absorption method is based on the principle that different gases absorb radiation at different amounts. For absorption tests, an infrared light is placed behind a sapphire window on the other side of the tube. This IR light source provides the sensor with a baseline IR emission reading. As different gases pass by the sensor, they absorb some of the IR light, resulting in a different level of IR signal at the sensor. Measuring the time at the absorption level that corresponds to the test gas corresponds to the test time within the

test section. Although the sensor is capable of reading the IR signal with this method, the emission method has provided more reliable measurements of test time. The emission method only allows for signal to come to the sensor when the test gas is passing by, whereas the absorption method also shows when the other gases pass by the sensor. A typical voltage trace of the absorption method is shown in Figure ???. It has been more difficult to measure test time with the absorption method than the emission method, so the emission method has been used primarily in the non-combusting tests and will continue to be used in the combustion tests. Further testing and tuning of the system is required to capture more meaningful information with this method.

### 3.4.4 Emission

The second method is infrared emission. As gases are heated, they emit IR radiation at different wavelengths. Using a filter, other wavelengths that are not these specific wavelengths, will not pass to the detector. For the non-reacting flows, a 5% CO<sub>2</sub> in nitrogen mixture emits IR within a 180nm bandwidth centered at 4.248 $\mu$ m. Placing the filter in front of the sensor allows the sensor to detect when, and for how long, the test gas, CO<sub>2</sub> passes by the sensor. Knowing how long the gas passes by the sensor allows for a direct measurement of test time in the test section. Due to the sensor's close proximity to the test section, the test time extracted from the IR data is very close to the test time for the models in the test section. An example of the voltage trace produced by the sensor using the emission method is shown in Figure ??.

Shown in the image are a few artifacts known about this system. Included in this voltage trace is the voltage of the pressure transducer at the same location as the IR sensor for reference. The sharp peak of the pressure signal indicates the arrival of the initial shock wave. This indicates that helium is flowing by at that time. However, there is an increase

in the IR signal. The current theory is that this signal is the presence of light produced by burning diaphragm particles flying down the tube. The next spike, however, is the  $CO_2$  passing by the IR source. Measuring the length of time this spike occurs over leads to the estimation of experimental test time.

### 3.4.5 Premature Ignition

The sensor will also be used to determine if pre-combustion occurred during a test. It is expected that if the reaction combusts upstream of the test section, it will result in a very large spike in IR signal. This will indicate that combustion did not originate at the cavity, but rather upstream of the cavity. Since the combustion tests are being used to test the flame-holding characteristics of the cavity, it is imperative that ignition originates at the cavity.

## 3.5 Schlieren Imaging

The images captured for the tests were done so using a high speed camera with a schlieren system. A diagram of the schlieren system at Lafayette can be seen in Figure 3.8. The camera used for image capturing is a Phantom Miro m310 camera, capable of taking images up to 100 fps. However, as the recording frame rate increases, the resolution of each image decreases. For testing, a nominal frame rate of 77,000 kHz was used, as this provided a sufficient frame rate without sacrificing too much resolution.

The schlieren effect operates on the principle that light refracts in air due to changes in density. This can be observed firsthand on a hot day. The rippling effect one can see above a road on a hot day is the light refracting due to the different densities of the air, caused by differences in local air temperature. Schlieren imaging takes advantage of this

principle by placing a knife edge at the focal point of the system. As light is refracted due to a change in density, this light gets blocked out by the knife edge, showing up as a dark spot in the captured image. Light that is not refracted continues through to the camera unblocked.

This type of imaging is important to see the various shock waves produced during testing. Since shock waves produce very sharp density gradients, a system that is capable of capturing these density gradients at high speeds is very useful. Typical test times experienced by the non-reacting tests were on the order of about 300 microseconds. With this camera, about 23 images were captured for the test time. With this many frames, it was possible to time correlate the images as well as extract dominant frequencies within the cavities.

Further information about the system, including more detail on how the system works and how to calibrate and align the system at Lafayette can be found in Ray Sanzi's honors thesis [14].

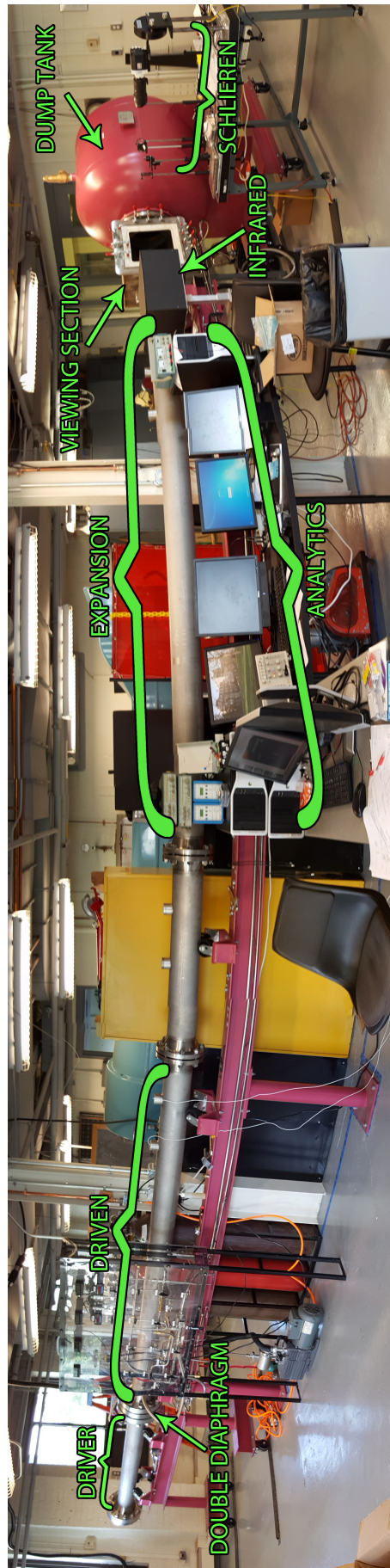


FIGURE 3.1: Annotated photograph of the expansion tube at Lafayette College

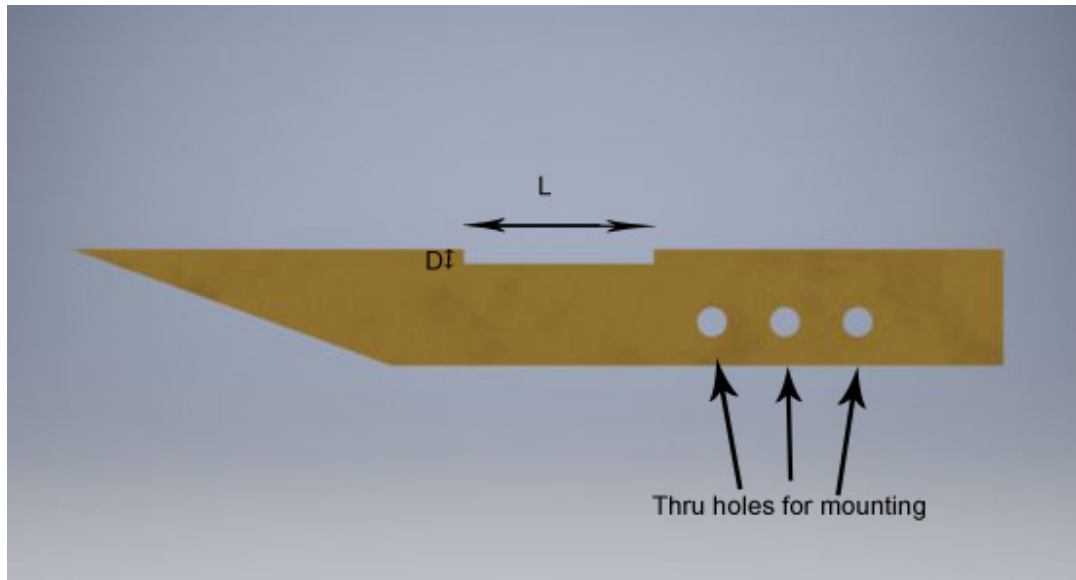


FIGURE 3.2: 3D rendering of cavity used in testing

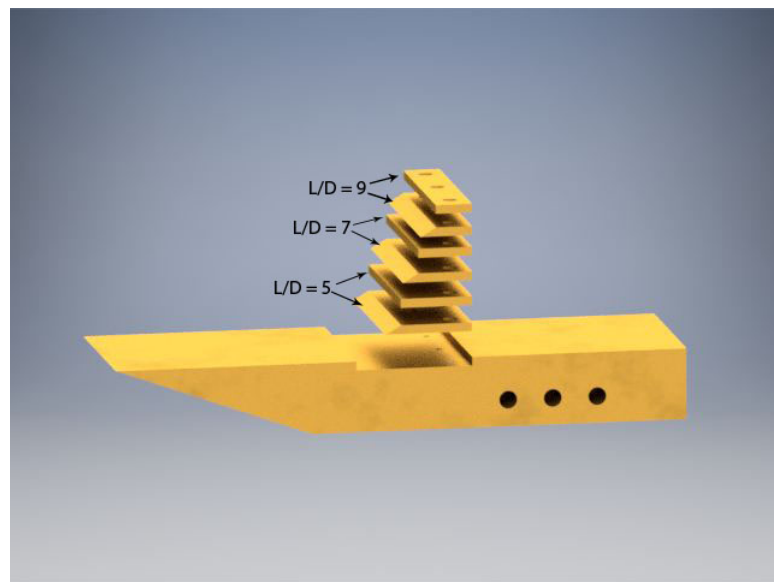


FIGURE 3.3: 3D rendering of cavity with various inserts to alter  $L/D$

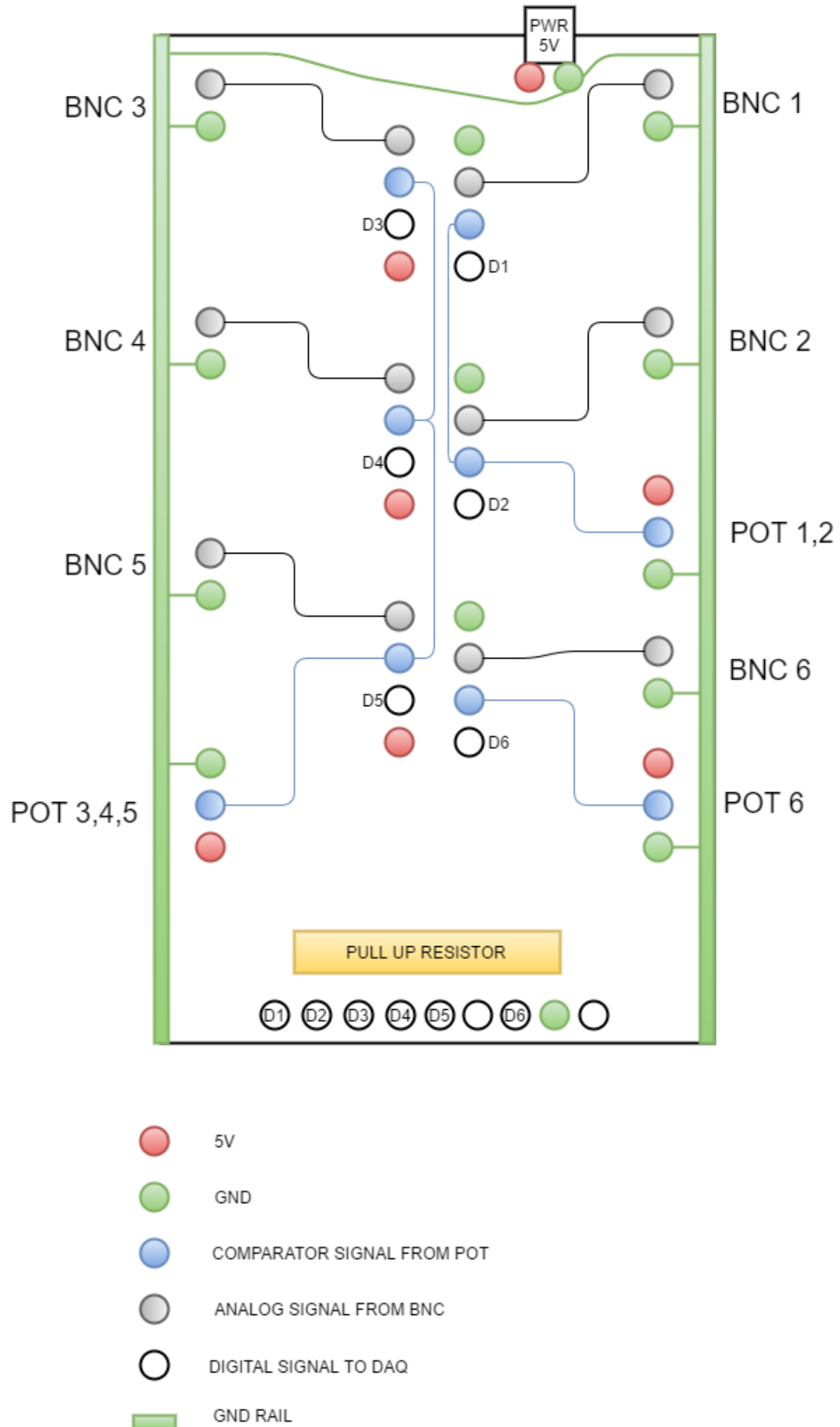


FIGURE 3.4: Circuit diagram for timer counter box

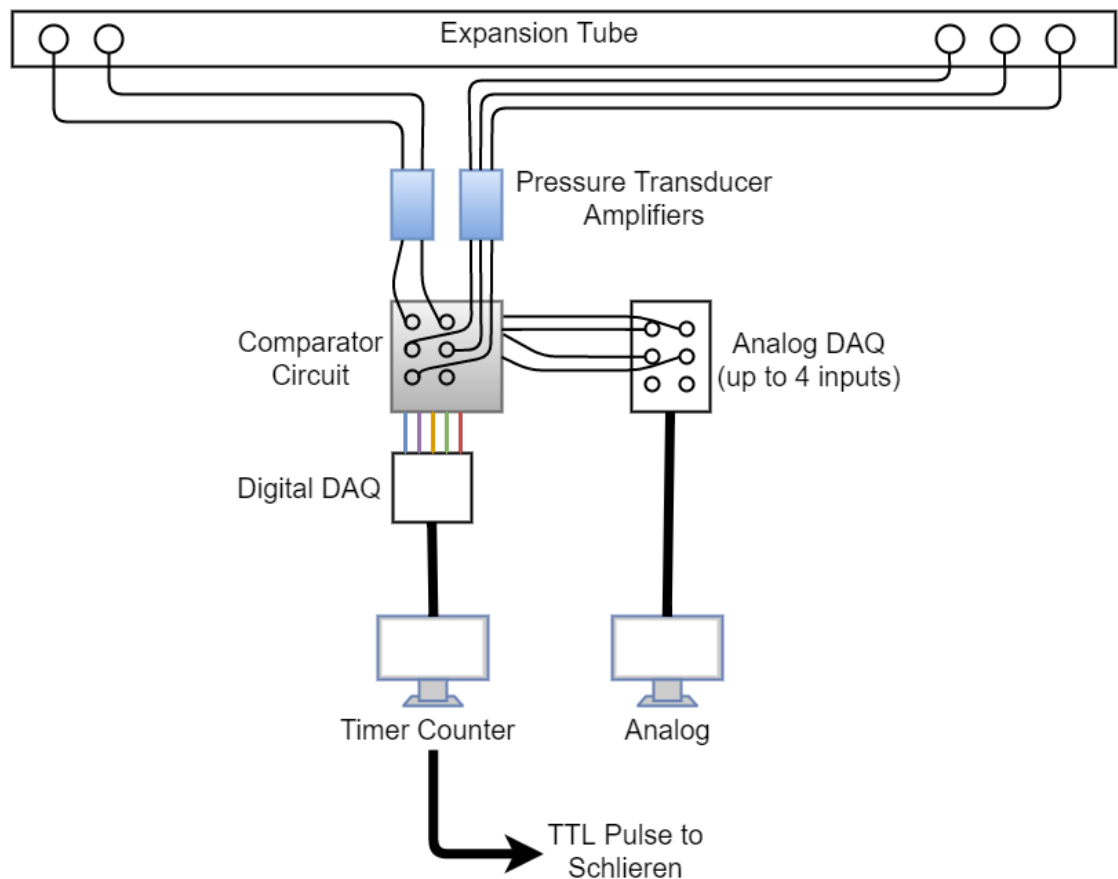


FIGURE 3.5: Data flow for high speed pressure transducers

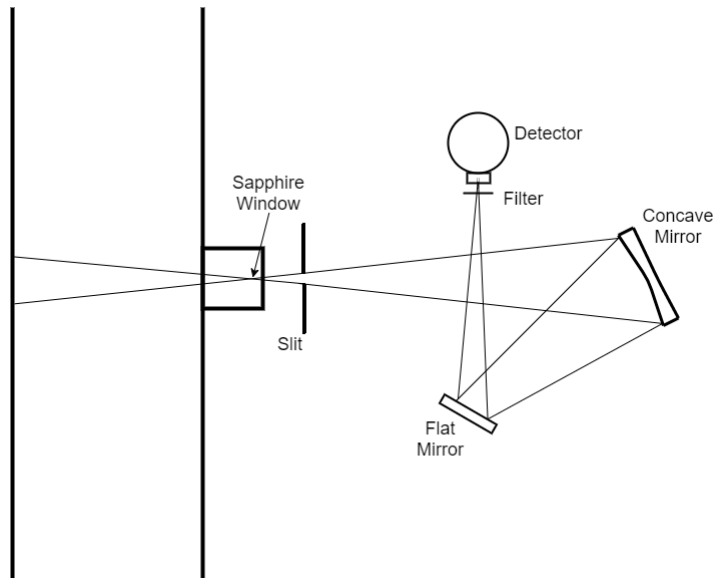


FIGURE 3.6: Schematic of the IR setup for the expansion tube.

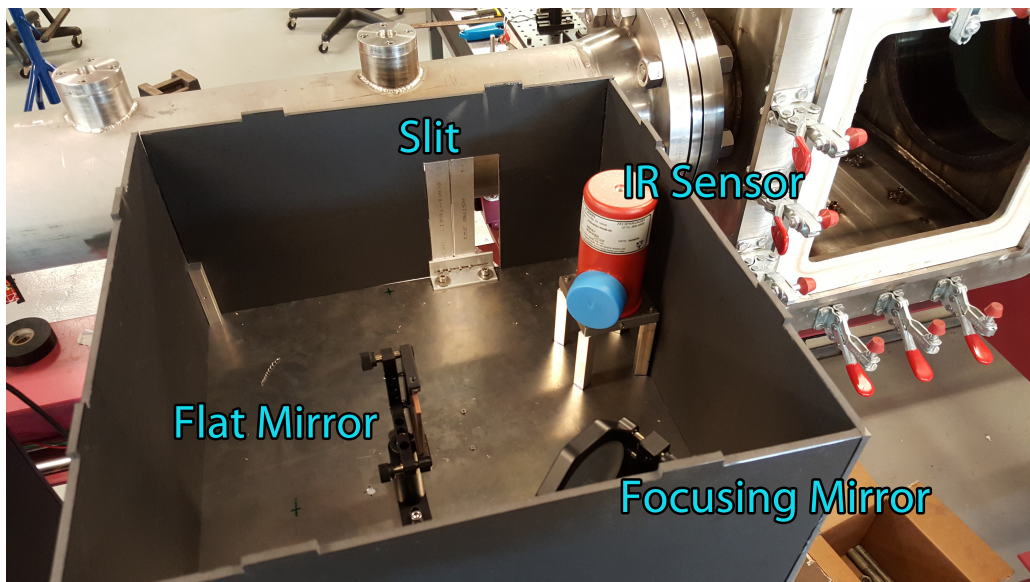


FIGURE 3.7: Photograph of actual IR setup in the lab.

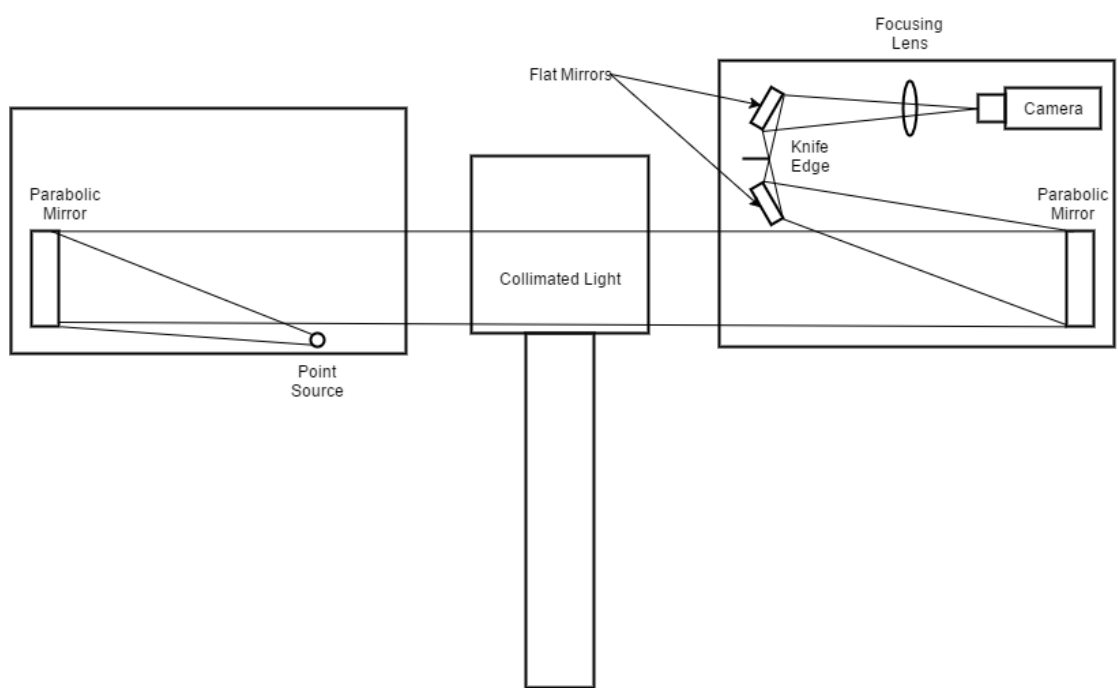


FIGURE 3.8: Diagram of schlieren system at Lafayette

## **Chapter 4**

# **Experimentation**

### **4.1 Phase 1**

#### **4.1.1 Setup and Conditions**

### **4.2 Phase 2**

#### **4.2.1 Setup and Conditions**

## **Chapter 5**

# **Experimental Results**

### **5.1 Phase 1 - Non-Combusting Tests**

#### **5.1.1 Schlieren**

#### **5.1.2 IR**

### **5.2 Combustion Tests**

#### **5.2.1 Schlieren**

#### **5.2.2 IR**

# **Chapter 6**

## **Future Work**

### **6.1 Phase 3**

### **6.2 Suggestions for Other Improvements**

#### **6.2.1 Pressure Transducers Within Cavity**

#### **6.2.2 Fuel Injection into Cavities**

# Bibliography

- [1] Adela Ben-Yakar. *Experimental investigation of mixing and ignition of transverse jets in supersonic crossflows*. PhD thesis, Stanford University, 2000.
- [2] Adela Ben-Yakar and Ronald K Hanson. Cavity flame-holders for ignition and flame stabilization in scramjets: an overview. *Journal of Propulsion and Power*, 17(4):869–877, 2001.
- [3] Hyungrok Do. *Plasma-assisted combustion in a supersonic flow*. PhD thesis, Stanford University, 2009.
- [4] Ibrahim Yilmaz, Ece Ayli, and Selin Aradag. Investigation of the effects of length to depth ratio on open supersonic cavities using cfd and proper orthogonal decomposition. *The Scientific World Journal*, 2013, 2013.
- [5] O Haldun Unalmis. Cavity oscillation mechanisms in high-speed flows. *AIAA Journal*, 42(10):2035–2041, 2004.
- [6] H Heller and J Delfs. Letter to the editor: cavity pressure oscillations: the generating mechanism visualized. *Journal of Sound and Vibration*, 196(2):248–252, 1996.

- [7] David R Williams, Daniel Cornelius, and Clarence W Rowley. Supersonic cavity response to open-loop forcing. In *Active Flow Control*, pages 230–243. Springer, 2007.
- [8] O Wayne McGregor and RA White. Drag of rectangular cavities in supersonic and transonic flow including the effects of cavity resonance. *AIAA Journal*, 8(11):1959–1964, 1970.
- [9] ShiBin Luo, Wei Huang, Jun Liu, and ZhenGuo Wang. Drag force investigation of cavities with different geometric configurations in supersonic flow. *Science China Technological Sciences*, 54(5):1345–1350, 2011.
- [10] N Sato, A Imamura, S Shiba, S Takahashi, M Tsue, and M Kono. Advanced mixing control in supersonic airstream with a wall-mounted cavity. *Journal of Propulsion and Power*, 15(2):358–360, 1999.
- [11] Stanford University. URL <https://web.stanford.edu/group/fpc/cgi-bin/fpcwiki/Main/Research>. [Online; accessed April 26, 2016].
- [12] Eli Lazar, Gregory Elliott, and Nick . Glumac. Control of the shear layer above a supersonic cavity using energy deposition. *AIAA journal*, 46(12):2987–2997, 2008.
- [13] Helen Hutchens. Theory, design, construction, and testing of an expansion tube. Master’s thesis, Lafayette College, 2015.
- [14] Raymond Sanzi III. Working title. Master’s thesis, Lafayette College, 2016.